
Article:
Yearby, K.H. and Pickett, J.S. (2022) A review of cluster wideband data multi-spacecraft observations of auroral kilometric radiation. Journal of Geophysical Research: Space Physics, 127 (2). e2021JA029499. ISSN: 2169-9380

https://doi.org/10.1029/2021ja029499

JGR Space Physics

REVIEW ARTICLE
10.1029/2021JA029499

Special Section:
Cluster 20th anniversary: results from the first 3D mission

A Review of Cluster Wideband Data Multi-Spacecraft Observations of Auroral Kilometric Radiation

K. H. Yearby[1] **and J. S. Pickett**[2]

[1]Department of Automatic Control and Systems Engineering, The University of Sheffield, Sheffield, UK, [2]Department of Physics and Astronomy, University of Iowa, Iowa City, IA, USA

Key Points:

- The Cluster spacecraft Wideband Data instruments have allowed important advances in the understanding of auroral kilometric radiation (AKR)
- Studies include source locations, angular beaming, and fine structure including pulsations and striations
- Similar AKR fine structures are sometimes observed simultaneously on the spacecraft and at ground level

Correspondence to:
K. H. Yearby,
k.h.yearby@sheffield.ac.uk

Citation:
Yearby, K. H., & Pickett, J. S. (2022). A Review of Cluster Wideband Data multi-spacecraft observations of auroral kilometric radiation. *Journal of Geophysical Research: Space Physics*, *127*, e2021JA029499. https://doi.org/10.1029/2021JA029499

Received 7 JUN 2021
Accepted 3 OCT 2021

Author Contributions:
Conceptualization: J. S. Pickett
Writing – original draft: K. H. Yearby
Writing – review & editing: K. H. Yearby, J. S. Pickett

Abstract We review important advances in the understanding of auroral kilometric radiation (AKR) resulting from observations by the Wideband Data instruments on the four Cluster spacecraft. AKR is an intense radio emission originating in the Earth's auroral regions with frequencies typically in the range 50–700 kHz, usually observed from space. It is now widely accepted that AKR is generated by the cyclotron maser instability (CMI) in density cavities in the auroral acceleration region. Multi-point observations by the Cluster spacecraft with a time delay of arrival technique have allowed the source locations of many individual AKR bursts to be determined. The position uncertainty is around 500 km at the source region or about 200 km when mapped on to the auroral zone. AKR is emitted in a narrow beam close to the tangent to the magnetic field vector in the source region. This has important implications for the possible generation mechanisms, being incompatible with filled or hollow cone beaming models. It also implies that an observer at a given location can only see AKR from a fraction of possibly active source regions. The complex frequency time structure of AKR sometimes shows regular striations or pulsations. Cluster observations of these phenomena have been interpreted as modulation of the CMI by disturbances propagating through the generation region. Exceptionally, AKR can sometimes be observed from low altitude spacecraft or even on the ground. Recent work has involved simultaneous observations of AKR on the Cluster spacecraft and on the ground at the South Pole.

Plain Language Summary A review of Cluster Wideband Data observations of auroral kilometric radiation (AKR). Multi-point observations have allowed the source locations of many individual AKR bursts to be determined. The angular beaming pattern was found to be close to the tangent to the magnetic field vector in the source region, which has important implications for the possible generation mechanisms. The complex frequency time structure of AKR sometimes shows regular striations or pulsations, which have been interpreted as modulation by disturbances propagating though the generation region. The most recent work has involved simultaneous observations of AKR on the Cluster spacecraft and on the ground at the South Pole.

1. Introduction

The first observations of auroral kilometric radiation (AKR) were probably those by Benediktov et al. (1965, 1968) on the Elektron-2 satellite. Although observations were made only at the highest part of the AKR spectrum (725 kHz), the observed emissions were clearly terrestrial with pronounced fluctuations in intensity observed at orbital distances less than 30,000 km from the Earth. They also showed a latitudinal variation with a minimum at the equator. Dunckel et al. (1970) observed AKR using the VLF receiver on the OGO 1 spacecraft. They referred to it as "high-pass" noise as the spectrum extended above the upper frequency range of the receiver. The noise was observed from a lower cutoff usually between 40 and 100 kHz, but sometimes as low as 20 kHz, mainly on the night side, and associated with magnetic storms. The source of the noise was not identified although it was suggested that it may be generated close to the Earth, as this could account for the approximate magnitude of the cutoff frequency.

The landmark paper by Gurnett (1974) described the first comprehensive study on the properties of AKR, then referred to as Terrestrial Kilometric Radiation, and its connection to substorms. The observations were made using radio wave experiments comprising 3 axis electric and magnetic antennae and filter bank spectrum analyzers onboard the Imp 6 and Imp 8 spacecraft. This basic instrumentation nevertheless allowed the main characteristics of AKR to be established.

The measured intensity of the radiation was modulated by the rotation of the antenna, with a deep minimum when the antenna null was aligned with the Earth. This indicated that the source had a small extent (<6° when viewed

from $32R_E$) and was within $3R_E$ of the Earth. Furthermore, the variation of the power flux was observed to follow the inverse square law, as expected for a compact source close to the Earth. The radiation was detected by both electric and magnetic loop antennae, with the ratio of the electric and magnetic field power spectral densities close to that expected for an electromagnetic wave in free space.

The occurrence of AKR showed a distinct low-latitude cutoff varying from about 40° magnetic latitude at $3.0R_E$ to about 10° magnetic latitude at $10.0R_E$. These results suggested that the AKR source must be at low altitude in the high-latitude region of the magnetosphere, with the cutoff resulting from absorption in the high density plasmasphere. AKR occurred in storms lasting from half an hour to several hours, closely related with discrete auroral arcs. The intensity of the radiation strongly depended on the magnetic local time and latitude of the spacecraft. At its most intense, the radiated power in the frequency range 50–500 kHz was estimated to be about 10^8 W.

Kurth et al. (1975) used direction finding observations on the Hawkeye 1 and Imp 8 spacecraft to determine that the AKR source was at altitudes between 1 and $2R_E$, in the evening sector (centered around 22 MLT). By averaging over AKR events lasting 1 hr or more the uncertainty in the measured direction was reduced to ±1° or less, which at a spacecraft distance of 23–$46R_E$, gives a source location uncertainty of 0.4–$0.8R_E$ (2,500–5,000 km).

The cyclotron maser instability (CMI) was proposed as the generation mechanism by Melrose (1976) and Wu and Lee (1979). The emission is excited by the CMI perpendicular to the magnetic field in deep density cavities associated with the auroral acceleration region. The waves are subsequently refracted by density structures into a beam closely aligned with the plane that is tangent to the magnetic field in the source region.

Gallagher and Gurnett (1979) used the Hawkeye 1 and Imp 6 spacecraft to determine the time averaged source location of AKR. Intense sources are found in both hemispheres near 65° invariant latitude, 22 to 24 MLT and near $2.5R_E$.

AKR has a complex frequency-time structure first reported by Gurnett et al. (1979) from observations by the ISEE-1 and ISEE-2 plasma wave instruments. They suggested this frequency time structure may be due to the sources ascending or descending on the magnetic field lines, with emission occurring at the electron cyclotron frequency at the source location.

The first interferometric measurements of AKR were reported by Baumback et al. (1986) providing information about the generation mechanism and source size, rather than source location. Electric field waveforms measured in a narrow bandwidth at 125 and 250 kHz by the ISEE 1 and ISEE 2 spacecraft were cross-correlated. The spacecraft separation, on a line perpendicular to the source, varied from 20 to 3,868 km, while the source — spacecraft distance was mostly greater than $10R_E$. Correlations exceeding 80% were observed even for the longest baselines. The authors argue that this shows the radiation must be coherent and that the source cannot be more than about 20 km in diameter.

Huff et al. (1988) determined the direction of arrival of strong AKR bursts received on the DE-1 spacecraft. By measuring the relative phase of the waves on two orthogonal electric field antennae as a function of the spacecraft spin, and assuming the waves are circularly polarized, both the azimuth and elevation can be determined to high precision. By further assuming emission occurs at the electron cyclotron frequency, they observed that the source locations were on field lines that mapped to features on auroral images taken by the same spacecraft.

Louarn et al. (1990) made the first in situ measurements in the AKR source region using a comprehensive set of wave and particle experiments on the Viking spacecraft. AKR source crossings are clearly observed as shown by a frequency minimum in the emission spectrum extending down to the electron cyclotron frequency (f_{ce}), together with an intensity enhancement. It is reported that detailed analysis of the electron distribution function supports a process where a trapped electron population, produced by a parallel electric field, drives the CMI and allows emission to occur over the observed AKR spectrum.

Knowledge of the AKR source region was further advanced by Ergun et al. (2000) using FAST spacecraft observations. They confirm the CMI as the generation mechanism with the important modification that AKR results from an unstable "horseshoe" electron distribution rather than a loss cone distribution. The instability results from electron acceleration by an electric field parallel to a dipole magnetic field. The electric field creates a density cavity within which the electrons have an energy from acceleration of a few keV and leads to a relativistic

correction to the electron cyclotron frequency ($f_{cr} = f_{ce}/\gamma$). This allows the generation of radiation at frequencies just below the local f_{ce}, as observed.

In this review paper of Cluster AKR results after 20 years in orbit, we first describe the spacecraft and instrumentation that made the observations. We then review the observations in three parts, the determination of source locations and angular beaming, investigations of the frequency/time structure of striated and pulsating AKR, and finally observations in the source region and on the ground.

2. The Cluster Spacecraft and Wideband Data Experiment

The four Cluster spacecraft were launched in two pairs in July and August 2000, into elliptical polar orbits with apogee up to $22R_E$. During AKR observations the separation between the spacecraft have varied from 2,000 km to more than 12,000 km. The spacecraft are spin stabilized at 15 RPM, and each spacecraft includes a pair of wire boom electric field antennae orientated in the spacecraft spin plane, measuring 88 m from tip to tip. Only one of these may be connected to the receiver at any time. However, as the orientation of the antenna changes with the spacecraft spin, some information on the polarization of the observed waves can be inferred.

The Wideband Data (WBD) experiment (Gurnett et al., 1997) makes high-resolution waveform measurements of a single field component up to 577 kHz. Frequencies above 77 kHz are handled in a frequency translation mode whereby a selected band is down-converted to baseband. The receiver provides three translation bands of 125, 250, and 500 kHz which are normally used in sequence to allow a wide frequency coverage. An automatic gain control system is used with an 8 bit analog to digital converter to provide a dynamic range greater than 100 dB. Data may be acquired in several sampling modes including a wide band (77 kHz) duty cycled mode or narrow band (9.5 or 4.2 kHz) continuously sampled mode. Telemetry may be acquired in real-time at 220 kbit s^{-1} or via the spacecraft solid state recorder at 73 kbit s^{-1}. In either mode a timing accuracy of around 20 μs is achievable.

A key reason for including WBD experiments on all Cluster spacecraft is to allow the location of remote sources to be determined by interferometry. An experiment to test this capability is described by Cummer et al. (2003). Rather than a natural radio wave source, the Radio Plasma Imager (RPI) experiment on the Image spacecraft is used as a transmitter. The experiment was performed on April 23, 2002, between 04:20 and 04:45 UTC. During this interval the Image — Cluster propagation distance varied from 3.6 to $2.7R_E$. The transmissions, with a power of ∼6 W, were received on all Cluster spacecraft throughout this time. Although the narrow bandwidth of the transmissions meant that the differential time delay technique ultimately used for determining AKR source locations could not be applied, the experiment did prove useful for Faraday rotation measurements.

3. AKR Source Locations and Angular Beaming

The first major Cluster AKR observations are described by Mutel et al. (2003). A novel technique is used which can determine individual AKR source locations with exceptional spatial and temporal resolution. These observations are made in a remote sensing mode where the spacecraft are located at a distance of around $10R_E$ above the polar cap. Along most of the path the wave frequency is much greater than the local plasma frequency so the AKR propagates to the spacecraft as a free space electro-magnetic wave.

The technique is based on the measurement of differential time delays from at least 3 locations in space. The time delays are determined by cross-correlating AKR burst waveforms observed on pairs of spacecraft. Although similar to the technique of Very Long Baseline Interferometry, only the differential time delays are used and not the interferometer phases (Mutel et al., 2004). The AKR waveforms are divided into frequency/time windows of typically 1 kHz bandwidth and 0.3 s duration, and cross-correlations performed for all such windows falling within an observation. Normally the cross-correlation function will contain one significant peak, with the time delay of the peak being the differential delay (Figure 1, reproduced from Mutel et al., 2003, figure 6). The uncertainty of this measurement is determined by the reciprocal of the AKR burst bandwidth and is typically around 0.3 ms. For a baseline in the range 5,000–10,000 km perpendicular to the source – spacecraft line, and a line of sight $6–12R_E$ between the spacecraft and the AKR emission, the position uncertainties perpendicular to the line of sight are 380–1,400 km at the location of the source. Even using four spacecraft, the uncertainty along the line of sight is large, so the altitude is determined by assuming that the frequency of the emission is equal to the electron

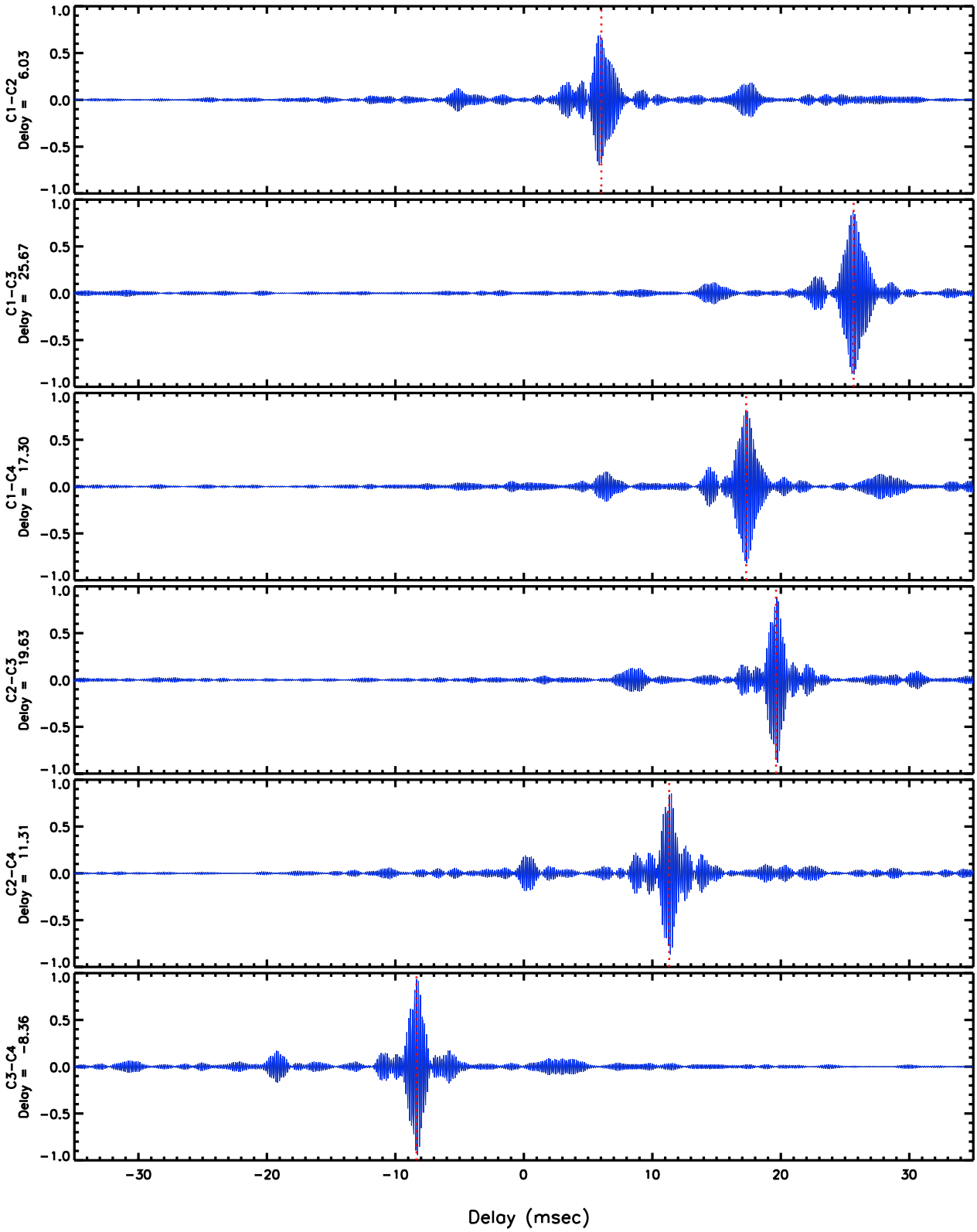

Figure 1. "Cross-correlation functions of Wideband Data waveforms received from all four cluster spacecraft on July 10, 2002 starting at 0846:53.04 UT. The waveforms were filtered in the time and frequency domain using windows of 300 ms and 1 kHz (506–507 kHz), respectively." Reprinted from Mutel et al. (2003), figure 6.

cyclotron frequency at the source location. When the estimated position is traced down the magnetic field line to 100 km altitude, the uncertainty is reduced by a factor of 2–3.

The source location algorithm is applied to all data windows which provide valid cross-correlation delays. The expected time delays at the spacecraft locations are computed from every point in a 3 dimensional grid centered on the Earth. All grid points where the expected and measured time delays agree to within the measurement uncertainty are included in the set of allowed positions. The positions are further constrained by keeping only those within one cell spacing of the surface where the electron cyclotron frequency is equal to the observed frequency. Finally, the centroid of the set of positions is taken as the position of that burst. Only a small proportion of data windows, typically a few percent, result in valid solutions. It is suggested this may be due to multiple AKR sources often illuminating the spacecraft at the same time.

The algorithm assumes propagation in a straight line from the source to each spacecraft. It is accepted that there are two situations where this may not be correct. First, there is a propagation distance of maybe 500 km upward from the generation region until the plasma density is low enough for free propagation to occur. This is not allowed for, so the source locations determined are for the region where free propagation begins. Second, the propagation may be subject to significant refraction due to the high density plasma in the plasmasphere. It is concluded that these propagation effects are not important for the observations reported in the paper, but could in principle be significant for low latitude paths ($\lambda_m < 30°$) at the lowest frequency (125 kHz).

The source locations of more than 1,700 AKR bursts are reported over six series of observations. As expected, the AKR sources are located on magnetic field lines connected to the night time auroral oval. In the north, burst locations tend to lie within the evening sector, while in the south they range from magnetic midnight to early morning.

Maps of the AKR source footprint locations for each epoch are shown in Figure 2 (reproduced from Mutel et al., 2003, figure 8). The footprints are distributed over an area measuring 1,000–2,000 km, much greater than the measurement uncertainty, but a small part of the auroral oval. At the time it was suggested that only this fraction had conditions suitable for AKR generation though later work concluded that AKR may be generated over a large part of the oval, but only a fraction of sources are observable from a given location in space due to beaming.

Mutel et al. (2008) made the first direct determination of the beam direction of individual AKR bursts. They use the tangent plane beaming model illustrated in Figure 3a (reprinted from Mutel et al., 2008), where the waves are generated perpendicular to the magnetic field by a "horseshoe" electron distribution in density cavities associated with the auroral acceleration region (Pritchett et al., 2002), and then refracted outward by density gradients in a beam aligned close to the magnetic field direction. In Figure 3b the calculated refraction angle versus horizontal distance at three frequencies is shown, using an approximate long-term average electron density profile.

The authors use the differential time delay technique of Mutel et al. (2003) to determine the source locations of more than 12,000 AKR bursts. For each burst, the coordinates of each spacecraft are then calculated in a 3-dimensional coordinate system centered on the source. In this system, x is parallel to the magnetic field direction, z at right angles to x in the magnetic meridian plane, and *y* completing a right handed set (Figure 3a). The "latitude" and "longitude" are then defined by analogy with standard geographic coordinates where the coordinate system xy plane is the equatorial plane, and *z* the polar axis. The distribution of spacecraft locations in this coordinate system is a measure of the beam width of the individual AKR bursts. This distribution is centered around 0° latitude, with more than 98% within ±20°. The distribution is around twice as wide in longitude with most within 40° of the origin. Note that this determination of the beaming pattern includes spacecraft locations with any detectable signal and may be somewhat wider than the half power beam width.

The implication for AKR generation mechanisms is nicely illustrated in Figure 4 (reprinted from Mutel et al., 2008). This compares visibility maps for the tangent plane beaming model and hollow cone models (Calvert, 1981). The visibility maps show all AKR source locations which could theoretically illuminate the four Cluster spacecraft if the emission is beamed according to each model. The tangent plane model has a width of 30° while the hollow cone models have opening angles of 20° and 40°. The AKR source locations determined from differential time delays (black x's and squares) fall almost entirely on the tangent plane beaming visibility

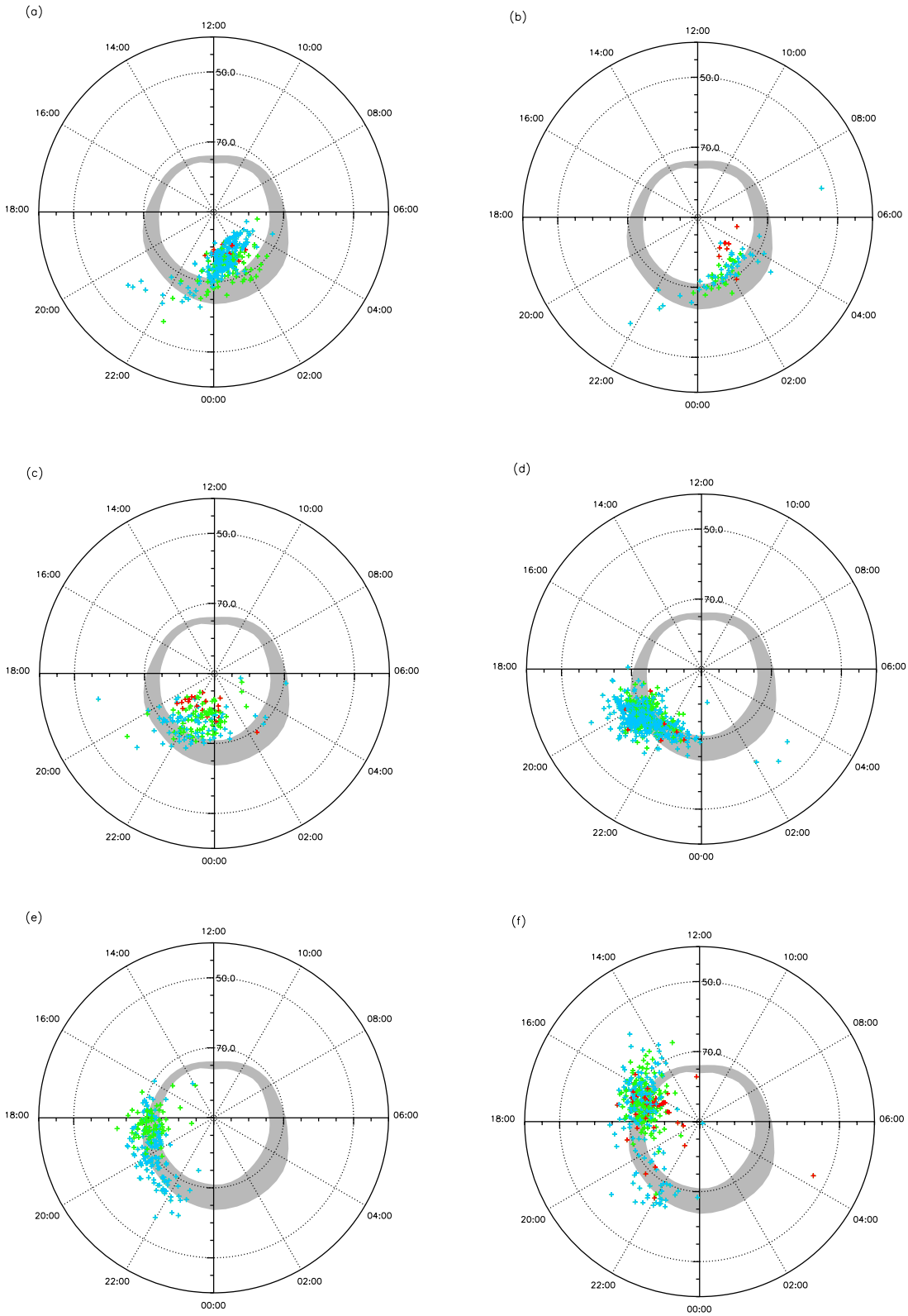
(a)
(b)
(c)
(d)
(e)
(f)
12:00
14:00
10:00
16:00
08:00
18:00
06:00
20:00
04:00
22:00
02:00
00:00
50.0
70.0

Figure 2.

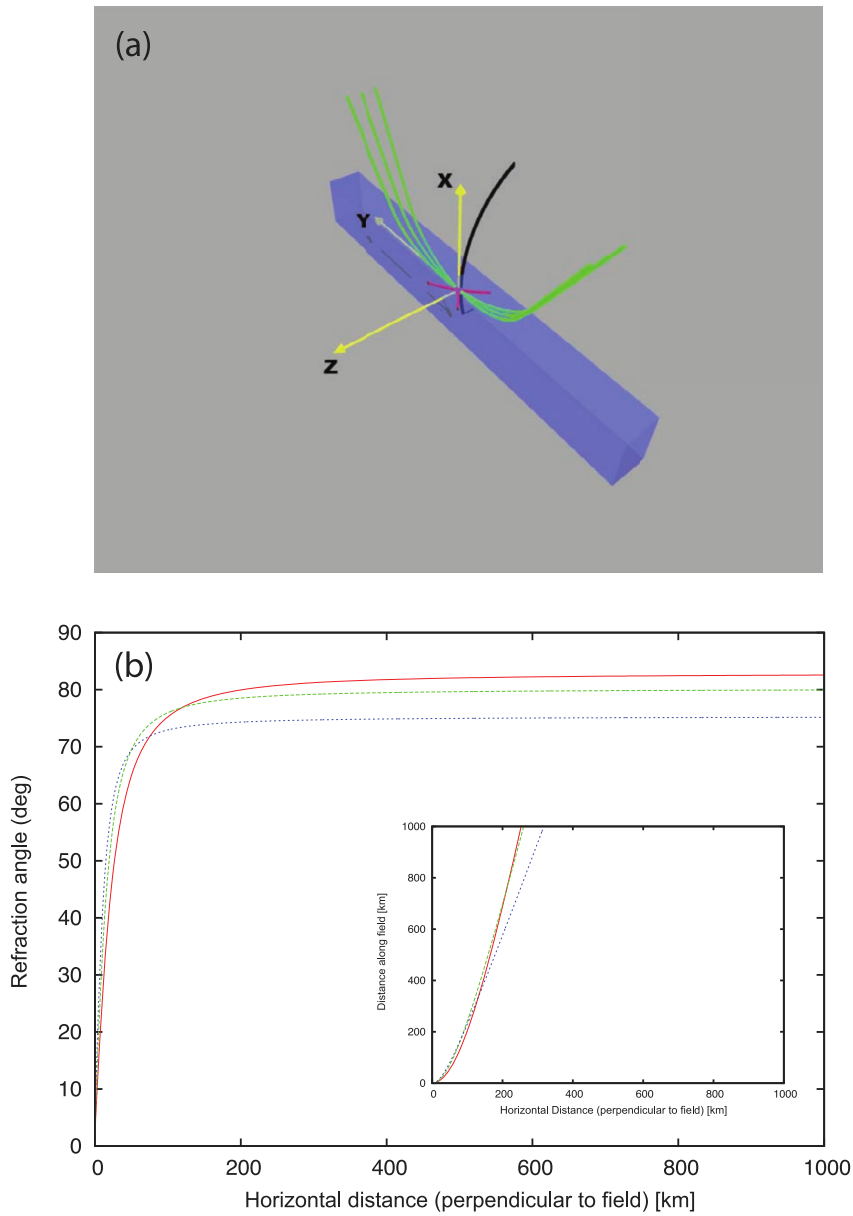

Figure 3. "(a) Geometry of the tangent plane beaming model. The tangent plane cavity, shown in blue, is tangent to a circle of constant latitude at the source. The green lines are escaping ray paths, the black line is the magnetic field, and the yellow arrows are the xyz coordinates system described in the text. (b) Refraction angle versus horizontal distance for rays at 125 kHz (red), 250 kHz (green), and 500 kHz (blue) initially perpendicular to the magnetic field. Ray paths are shown in the lower right inset." Reprinted from Mutel et al. (2008), figure 1.

map (yellow), and clearly do not fit either of the hollow cone models. This beaming pattern implies that only a fraction of active AKR sources can be observed from a given remote location. It also allows a re-interpretation of previous Cluster studies of AKR source locations (Mutel et al., 2003) which are now understood to be only a fraction of the possibly active source locations.

Figure 2. "Auroral kilometric radiation burst positions observed at each epoch as a function of corrected geomagnetic coordinates. A statistical auroral oval (gray) is superposed for reference, based on the model of Feldstein and Starkov (1967) for a moderate Kp index. Each cross is the centroid of solutions for an individual AKR burst at 125–135 KHz band (red crosses), 250–260 KHz band (green crosses), and 500–510 KHz band (blue crosses). Epoch labels are (a) July 10, 2002 (Southern Hemisphere), (b) July 17, 2002 (Southern Hemisphere), (c) August 19, 2002 (Southern Hemisphere), (d) November 9, 2002 (Northern Hemisphere), (e) December 29, 2002 (Northern Hemisphere), and (f) January 22, 2003 (Northern Hemisphere)." Reprinted from Mutel et al. (2003), figure 8.

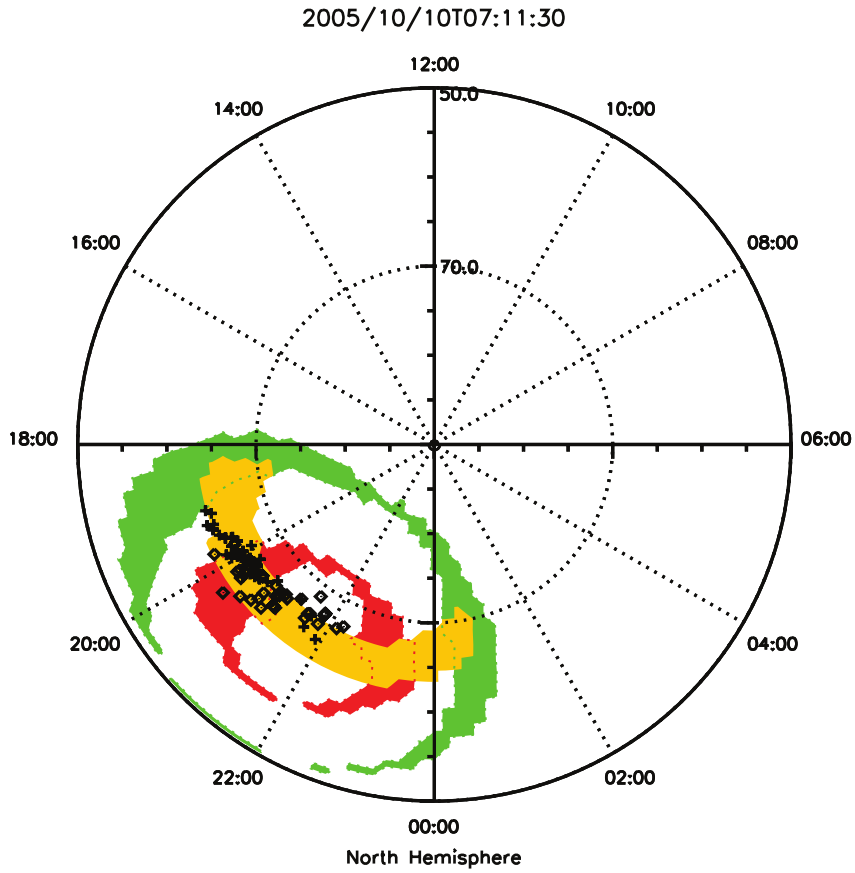

Figure 4. "Comparison of visibility maps for tangent plane beaming model (0°–45° longitude, 0° ± 15° latitude, yellow) with 20° wide hollow cone models (opening angles 20° (red) and 40° (green)) for the 4-spacecraft Cluster array on October 10, 2005 at 07:11 UT. The locations of auroral kilometric radiation burst source determined from differential delay solutions are shown as black x's (125 kHz), and squares (250 kHz)." Reprinted from Mutel et al. (2008), figure 4.

4. Striated and Pulsating AKR

As first reported by Gurnett et al. (1979), AKR has a complex frequency-time structure. Often this has the form of emissions of narrow bandwidth and slowly drifting frequency that appear fairly random (see for example Figure 5 above 180 kHz). Less commonly, striated emissions with rapidly changing frequency (below 180 kHz in Figure 5) or pulsating emissions are observed. The following works interpret these striations or pulsations as modulation of the CMI by a disturbance (ion solitary structures, electromagnetic ion-cyclotron (EMIC) wave or Alfvén wave) propagating through the generation region, with the frequency drift determined by the velocity of the disturbance.

Mutel et al. (2006) studied 651 individual striated AKR bursts observed by Cluster during 2002–2005. They report striated AKR to be a rare phenomenon with an occurrence of around 0.2% in the 125–135 kHz band, and less than 0.01% in the 500–510 kHz band. This compares to an occurrence of around 30% for non-striated AKR.

The frequency drift is typically in the range -2 kHz s^{-1}–-8 kHz s^{-1}. Assuming emission occurs at the electron cyclotron frequency at the source, this may be interpreted as the source moving upwards along the magnetic field line at 75–300 km s^{-1}. Striated AKR has an unusually narrow bandwidth, typically around 20 Hz, when detrended by a signal of constant negative slope. Using this bandwidth the authors estimate the source extent in the magnetic field direction to be 0.76 km, and state: "This is considerably smaller than the lateral extent of the AKR source region and indicates the trigger for SAKR must have a dimension along the magnetic field of order 1 km". Further, by comparing the observed intensity on multiple spacecraft, the beam width (full width and half power) of individual bursts is estimated to be around 5° in the 125 kHz band.

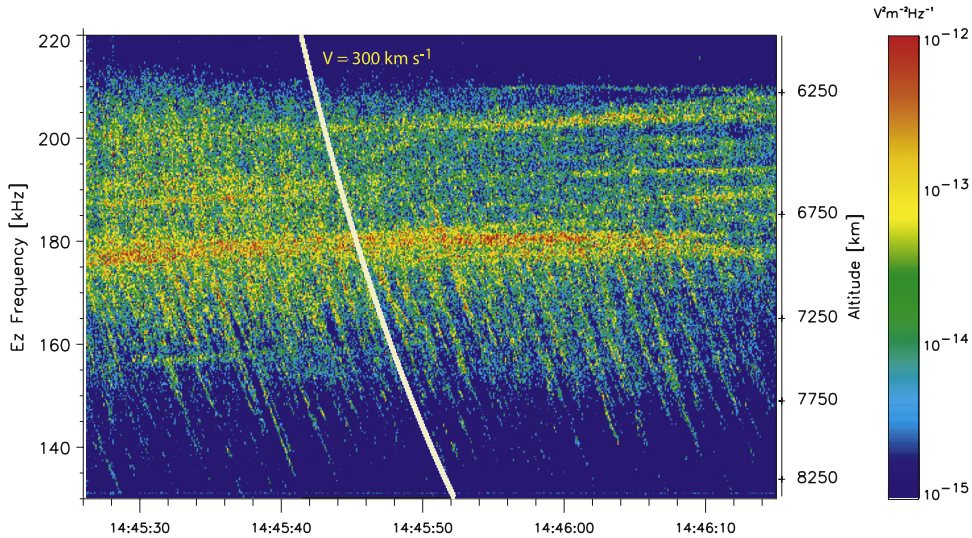

Figure 5. "Striated auroral kilometric radiation (AKR) bursts observed on Cluster spacecraft SC2 on January 15, 2005 from 1,445:26 to. 1,446:15 UT. Individual burst trails extend from 180 to 135 kHz, corresponding to an altitude range from 7,000–8,100 km. The yellow line is a calculated trail for a constant velocity source moving upward at 300 kms^{-1}. Note that the SAKR bursts appear to originate at or near an intense, slowly drifting AKR source at ~7,000 km." Reprinted from Mutel et al. (2006), figure 4.

The observed frequency slope, bandwidth and angular beam size are all reported to be consistent with triggering of the emission by ion solitary structures moving upward along the field line. Ion solitary structures are regions of localized ion density depletion associated with upward going ion beams. The authors suggest that a passing ion solitary structure may perturb the horseshoe electron distribution function driving the CMI resulting in a strong enhancement of the growth rate, and hence AKR emission at the structure location.

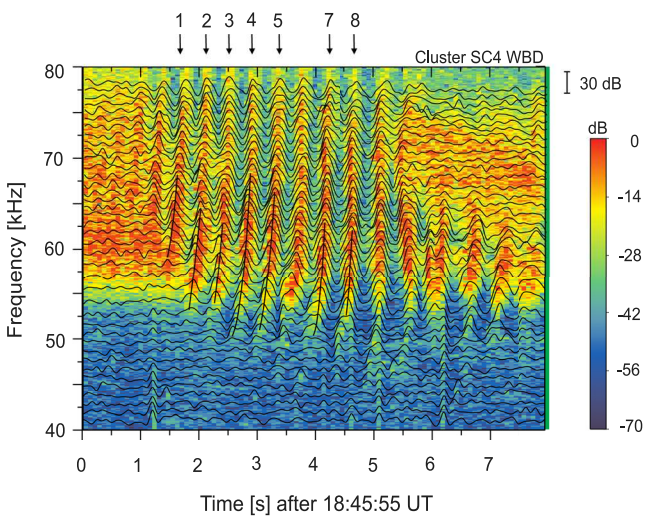

Figure 6. "High resolution FFT (2,180 points) frequency time spectrogram of auroral kilometric radiation pulsating at the Pc1 frequency, obtained from the SC4 Cluster satellite on June 22, 2003 18h45m55s UT. Overlaid are stacked intensity profiles in logarithmic scale, averaged over 1 kHz equivalent to a bandwidth of 10 successive frequency steps of the FFT spectrogram (obtained from 2,180 data points). The nearly vertical lines associated with selected pulses are quadratic regressions through maxima of pulse intensity. Position of the satellite: distance from the Earth 12 Earth's radii, magnetic local time (MLT) 6.9 hr, magnetic latitude −71.5°." Reprinted from Hanasz et al. (2008), figure 1.

If striated AKR bursts are indeed stimulated by ion solitary structures, then these observations provide a new technique to study these structures. The 45 kHz frequency range of the striated AKR bursts in Figure 5 imply that the associated ion solitary structures propagate upward for 1,100 km, with a lifetime of around 5 s, characteristics that could not be measured in situ with a single spacecraft.

Menietti et al. (2006) suggest striated AKR may be stimulated by upward traveling EMIC waves. An event was studied during an approximate conjunction between the Cluster and Polar spacecraft. In-situ particle data near the top of the AKR source region (f_{ce} = 50 kHz) was obtained by Polar about 20 min before Cluster wave observations at higher altitude above this region. Modeling of EMIC wave generation by the particle distribution observed by Polar suggest it is possible that such waves stimulated the observed striated AKR. However, as this was not a perfect conjunction, the EMIC waves could not be observed directly.

Hanasz et al. (2008) used the Cluster WBD experiment to study an unusual phenomenon where AKR is observed to pulsate at Pc1 frequencies (1–4 Hz). Just 15 events were found over 5 years of observations, with all but one of them occurring on May 16, 2005, between 13:25 and 14:50 UTC, in the recovery phase following a strong magnetic storm. The paper studies the separate event shown in Figure 6 (from Hanasz et al., 2008, figure 1), observed on June 22, 2003 at 18:46 UTC. This event was chosen for its unusual regularity and measurable frequency drifts. The other events were at higher frequencies

with frequency drifts too fast to measure. The AKR pulses have rapidly increasing frequencies, which correspond to downward motion of the source at velocities (3,000–15,000 km/s) matching the calculated velocity of Alfvén waves in the auroral cavity.

The authors suggest that the AKR pulsations may be caused by EMIC waves generated in either the equatorial magnetosphere or the auroral cavity which are then converted to Alfvén waves. In any case, it is assumed that Alfvén waves at the pulsation frequency are present at altitudes of 11,500–13,500 km within the auroral cavity. They state: "These waves can periodically accelerate electrons on auroral field lines to energies of several keV and modify the "shell" electron distribution in the converging magnetic field, which is needed for generation of pulsating AKR through the electron CMI."

It is suggested that the rarity of AKR pulsations at Pc1 frequencies may be explained given that Pc1 pulsations mainly occur on the dayside while AKR occurs mainly on the nightside. However there is some overlap between Pc1 geomagnetic pulsations in the afternoon sector and AKR occurrence in the evening sector. The source location of the event subject to this case study is not known, being observed by a single spacecraft at high latitude with visibility of the whole auroral oval.

Pottelette and Pickett (2007) and Pottelette et al. (2014) studied the relationship between AKR fine structure and phase space holes. Although using mainly FAST data, they use one Cluster event from the May 16, 2005 interval identified by Hanasz et al. (2008) above. This remarkable event shows both pulsations and striations at the same time. Pulsations are observed at frequencies above a boundary f^* at about 70 kHz, with striations below. Pottelette and Pickett (2007) state: "These observations can be interpreted as the result of a local acceleration by a pulsing parallel electric field layer located at a quasi-steady altitude of ∼11,000 km for which the value of the electron cyclotron frequency is f^*." Above this layer (at $f_{ce} < 70$ kHz) the slope of the AKR striations corresponds to a speed of 210 km/s which is typical for upward propagating ion holes. Downstream of this layer (at $f_{ce} > 70$ kHz) electron holes propagating earthward at high speed drive the pulsations.

For these Cluster studies of AKR modulation, no direct simultaneous measurements of the associated disturbances have been made. This is not surprising as AKR is normally observed in a remote sensing mode where the spacecraft are at a considerable distance from the AKR source and not even on the same field line, while conjunctions with other missions or ground stations are rare. However, Uozumi et al. (2011) reported a temporal correlation between Pi2 pulsations (∼1 min period) observed on the ground and the AKR power observed on the Polar spacecraft.

5. Observations in the Source Region and at Ground Level

By 2009, evolution of the Cluster orbit to lower perigee heights allowed observations within the auroral acceleration region (the AKR source region). Mutel et al. (2011) report the first multi-spacecraft observations of AKR in the auroral acceleration region allowing the identification of the wave modes and plasma parameters. To help understanding of these results we briefly review wave propagation in a cold, magnetized plasma. There are four modes that can propagate, the LO and W (ordinary) and RX and Z (extraordinary) modes. The low densities in this region preferentially support wave growth in the extraordinary modes though the LO mode is sometimes observed (Hanasz et al., 2003). At frequencies below the upper hybrid resonance (f_{uhr}) waves propagate in the Z mode. Above f_{uhr} is a small gap below the RX mode low frequency cutoff, f_{rx}, where neither mode propagates. Both f_{uhr} and f_{rx} depend on the magnetic field and electron density, such that $f_{rx} > f_{uhr} > f_{ce}$. The Z mode is normally trapped in the plasma, since waves propagating upwards will encounter the f_{uhr} cutoff before reaching free space, hence it can only be observed in-situ below the f_{uhr} level.

Cluster observations of waves in the Z and RX modes are reported. Results from 12 December 2009 are shown in Figure 7 (adapted from Mutel et al. (2011), figure 3). The gap between the RX mode (above) and Z mode (below) are clearly visible on the C3 and C4 spectra. These spacecraft are in similar orbits with C3 approximately 3 min behind. The electron cyclotron frequency derived from the spacecraft magnetometer is shown as a dashed line, with f_{uhr} defining the Z mode upper cutoff just above. Electron density measurements indicate the spacecraft entered a rather broad density cavity at around 04:30 until 04:45 UTC. Even within this cavity the density is relatively high, around 20 cm^{-3}, leading to an f_{pe}/f_{ce} ratio of 0.13.

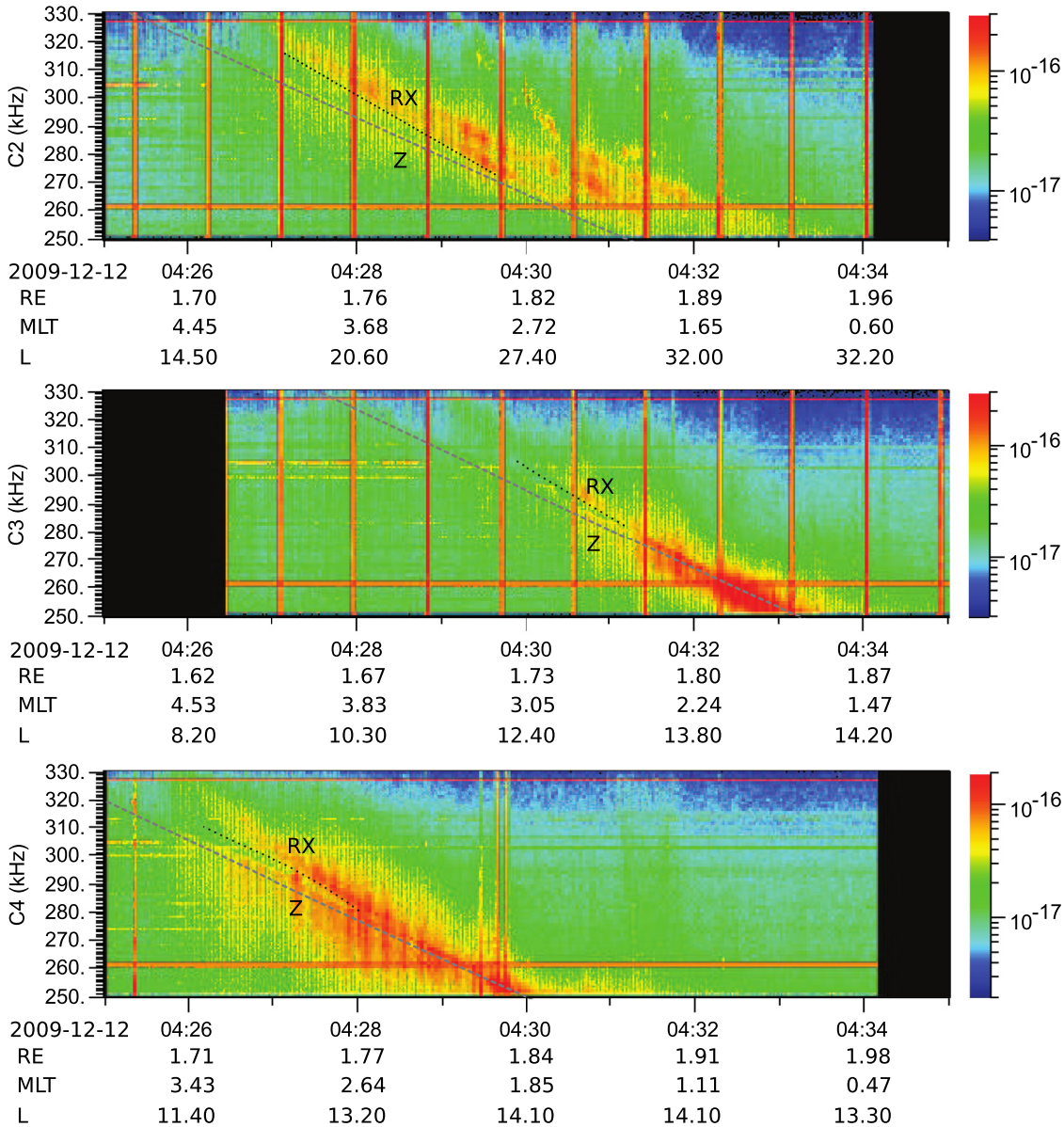

Figure 7. Cluster Wideband Data spectrograms observed at spacecraft C2 — C4 on December 12, 2009 from 04:25 to 04:35 UTC. The RX-Z mode gap is marked by dotted lines. This is most visible on C3 and C4 spectra, which are similar but offset by 3 min according to the orbits. The dashed lines mark the local electron cyclotron frequency at each spacecraft determined by the magnetometer. The spacecraft positions as R_E, magnetic local time and L value are marked. The color scale is power spectral density in $V^2m^{-2}Hz^{-1}$. Adapted from Mutel et al. (2011), figure 3, with permission of Austrian Academy of Sciences Press.

The authors compare the observed cutoff frequencies f_{uhr} and f_{rx} with estimates derived from local measurements of the magnetic field and electron density. Overall there is good agreement, though on short timescales there are some differences, particularly for the RX mode. They suggest this could be due to a less distinct RX mode cut off frequency in the observations or a warm plasma correction to the theory.

The growth rates of the Z and RX modes and hence the relative intensities of the observed waves depend on the ratio f_{pe}/f_{ce} (Mutel et al., 2011 use the symbol β to describe this ratio, which is not the same as the commonly defined plasma beta, the ratio of the plasma pressure to the magnetic pressure.). The authors report that the similar observed intensities of the two modes and relatively high f_{pe}/f_{ce} ratio are consistent with a model where the Z mode is generated at the source in preference to one involving mode-conversion at cavity boundaries, such as that by Pritchett et al. (2002). This is an important result when considering possible mechanisms allowing AKR to be

observed at low altitudes or on the ground. This situation contrasts with Viking observations reported by Louarn et al. (1990) with a density of 0.7 cm^{-3}, an f_{pe}/f_{ce} ratio of 0.04 and little if any Z mode waves observed.

It should be noted however that the intensities of both Z and RX modes observed by Mutel et al. (2011) are rather low at around 3×10^{-16} $V^2m^{-2}Hz^{-1}$.This compares to AKR source region intensities of 5×10^{-7} $V^2m^{-2}Hz^{-1}$ or more from FAST observations reported by Ergun et al. (2000), and an average spectral power of 10^{-8} $V^2m^{-2}Hz^{-1}$ quoted by Mutel et al. (2007). It suggests that in this case growth rates for both modes were substantially lower than typical for AKR sources. This may again be due to the higher plasma density during the Cluster observations compared to Viking or FAST. It is also possible that the Cluster observations were not local to the source.

Although AKR is usually observed in space at great distances from the Earth, there have been some reports of emissions resembling AKR at low altitude and on the ground (for example LaBelle et al., 2015; Parrot & Berthelier, 2012). To further explore this issue LaBelle et al. (2022) conducted a campaign of simultaneous observations on the Cluster spacecraft and on the ground at South Pole. They suggest that the key to explaining AKR observations at ground level is that Z-mode radiation generated in the source region can convert to the whistler (W) mode. This can occur through refraction on density and magnetic field gradients, via scattering on irregularities, or through nonlinear mechanisms. The whistler mode can propagate long distances and under favorable conditions through the ionosphere to be observed at ground level. They refer to AKR that reaches the ground in this way as "leaked". While the escaping and leaked AKR originate in different modes (RX and Z) in the source region, it is expected that the two modes are generated at the same time by the same unstable electron distribution, both within a narrow band just below f_{ce}, so similar fine structure features should be observed in each mode. Observing this coincident fine structure is difficult in practice given that many AKR sources are active simultaneously, and different subsets of these are potentially visible to observers in space and on the ground.

Observations were targeted when AKR was most likely to be observed at both locations that is during the austral winter when the Cluster spacecraft were at high southern latitudes and around magnetic midnight at South Pole. More recently the tangent plane beaming model (Mutel et al., 2008) was used to further constrain observations to times when Cluster was most likely to observe AKR visible from South Pole. A total of 90 hr of coordinated observations were scheduled over the austral winters of 2018–2020. During these observations AKR was observed ∼5% of this time at South Pole and ∼30% on Cluster. Cluster observations were made in a mix of wideband and narrow band modes, the former being most suitable for comparing the fine structure with that at South Pole, and the latter allowing AKR sources to be located using the method of Mutel et al. (2003). Observations at both locations often show qualitatively similar AKR fine structure.

More rarely, almost identical fine structure has been observed, comprising about 0.1%–0.3% of the AKR observed on Cluster during the coordinated observations, and ∼2% of the AKR observed at South Pole when Cluster was observing the appropriate frequency range. For example, in the event shown in Figure 8 (reprinted from Labelle et al., 2022) on June 29, 2020, between 03:17:00 and 03:17:20 a rising frequency structure from 500 to 580 kHz is seen. Although no such correlation is seen after 03:18, it is entirely possible that the AKR observed on Cluster at this time is from a different source, not visible from South Pole. Differential time delay measurements on Cluster put the footprint of the AKR source field line during this event at around 1,000 km from South Pole, within the range of sub-ionospheric propagation from the exit point to the receiver.

For this event, the power spectral density observed by cluster is 1 $\mu V^2m^{-2}Hz^{-1}$ and (assuming emission into a 20° beam width) the estimated radiated power of the AKR source is 170 kW, while that of the AKR observed at South Pole is just 35 mW assuming an illuminated region 1,000 km in diameter on the ground. This suggests that the generation of leaked AKR is a relatively inefficient process. This suggestion is also supported by observations from low altitude spacecraft. Parrot and Berthelier (2012) report leaked AKR maximum intensities of the order of 1 $\mu V^2m^{-2}Hz^{-1}$ on the Demeter spacecraft at 700 km altitude. Escaping AKR with similar intensities are observed on Cluster at around 30 times greater distance from the source, implying a much greater radiated power.

6. Conclusions and Suggestions for Future Work

Multi-point observations by the Cluster spacecraft using a differential time delay technique have allowed the source locations of 1,700 individual AKR bursts to be determined during six epochs in 2002 and 2003 (Mutel et al., 2003, 2004). The position uncertainties perpendicular to the line of sight are 380–1,400 km at the source

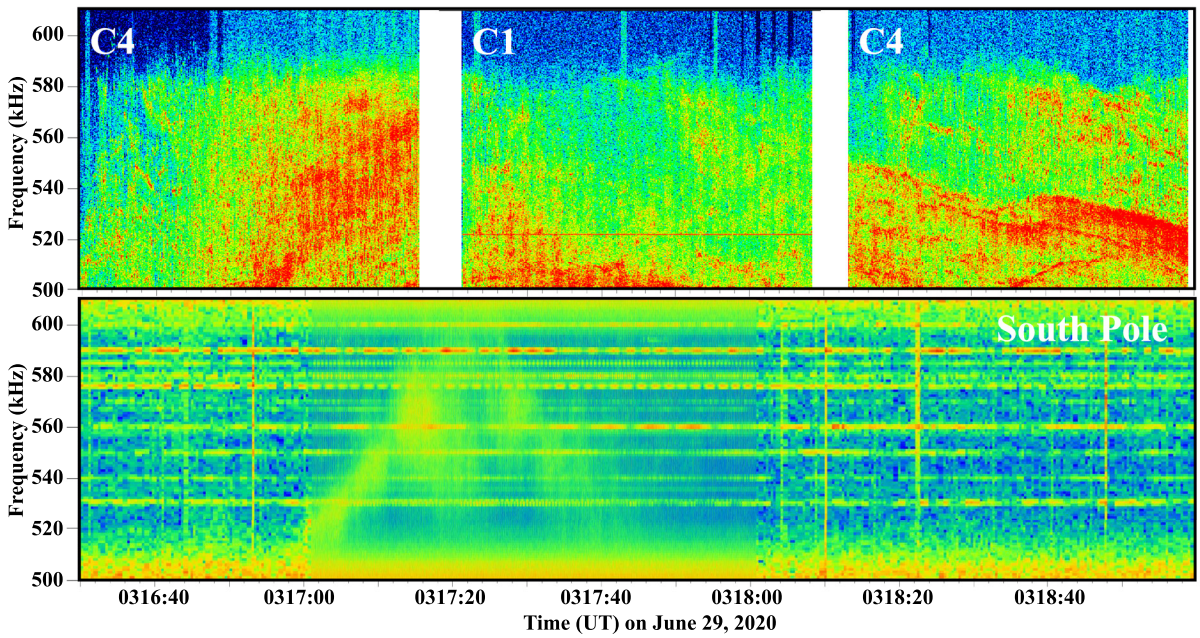

Figure 8. "500–610 kHz spectrograms of escaping auroral kilometric radiation (AKR) observed with the Cluster C1 and C4 satellites (top panel) and leaked AKR observed at South Pole Station (bottom panel)." Reprinted from LaBelle et al. (2022), figure 6.

location, which is reduced by a factor of 2–3 when traced along the field line to 100 km altitude. Comparing the source to spacecraft direction with the magnetic field direction in the source region, Mutel et al. (2008) determined the angular beaming pattern of more than 12,000 individual AKR bursts. These observations show that AKR bursts are beamed in a narrow plane tangent to the magnetic field direction at the source, and that this beaming pattern is not consistent with filled or hollow cone models. This beaming pattern also implies that only a fraction of active AKR sources can be observed from one remote location.

The rare phenomenon of striated or pulsating AKR has been the subject of several Cluster studies (Hanasz et al., 2008, Menietti et al., 2006, and Mutel et al., 2006). All suggest that the AKR structure may result from modulation of the CMI by a disturbance (ion solitary structures, EMIC wave or Alfvén wave) traveling through the generation region. Mutel et al. (2006) suggest that observations of striated AKR could be used to infer characteristics of ion solitary structures that cannot be measured in situ with a single spacecraft.

However, no direct simultaneous observations of the associated disturbances were made as part of these studies. This is not surprising as AKR is normally observed in a remote sensing mode where the spacecraft are at a considerable distance from the source. An opportunity to perform such measurements may occur during the Cluster mission extension in 2023/2024 when Cluster 2 will pass through the auroral acceleration region while the other spacecraft are at higher altitudes. This configuration differs from the low altitude passes earlier in the mission when the spacecraft were close together.

By 2009, evolution of the Cluster orbit allowed observations within the AKR source region (the auroral acceleration region). Mutel et al. (2011) report the first multi-point in-situ measurements of AKR in this region allowing the identification of the wave modes and plasma parameters. Again, the Cluster mission extension may allow an extension of this work by permitting simultaneous in situ and remote observations. As suggested by one of the referees, the work would be much enhanced by including measurements of parallel electric fields and electron distribution functions to characterize the AKR source.

LaBelle et al. (2022) report simultaneous observations of AKR on the Cluster spacecraft and on the ground at South Pole which, on rare occasions, show matching fine structure. It is suggested that escaping and leaked AKR originate in different modes (X and Z) in the source region, with the Z mode then converting to whistler mode which can under suitable conditions propagate to the ground.

An incidental feature in the spectrogram in Figure 7 suggests it may be possible to study wave propagation from the source region to the ground in reverse, with the advantage of a constant controlled source. At 300 and 305 kHz extending from the start to just before the dashed line marking the local electron cyclotron frequency are what appear to be signals from ground based LF transmitters (other horizontal lines, including at 262 and 327 kHz are local interference). Over the full duration of these low altitude observations (beyond that shown in Figure 7, but available from the data archives referenced below) signals from transmitters with frequencies ranging from 24 kHz to over 500 kHz are seen. Whilst the Cluster WBD experiment uses only a single antenna, the variation of the signal amplitude and phase as a function of the spacecraft spin allow determination of the wave polarization ellipse projected onto the spacecraft spin plane, and hence some information on the wave mode.

Conflict of Interest

The authors declare no conflicts of interest relevant to this study.

Data Availability Statement

The Cluster WBD data and spacecraft location data used in the reviewed works are available at the Cluster Science Archive, URL www.cosmos.esa.int/web/csa and at the NASA Coordinated Data Analysis Web, URL cdaweb.gsfc.nasa.gov.

Acknowledgments
K.H. Yearby acknowledges support from the UK Science and Technology Facilities Council grant ST/R000697/1.

References

Baumback, M. M., Gurnett, D. A., Calvert, W., & Shawhan, S. D. (1986). Satellite interferometric measurements of auroral kilometric radiation. *Geophysical Research Letters*, *13*, 1105–1108. https://doi.org/10.1029/GL013i011p01105

Benediktov, E. A., Getmantsev, G. G., Mityakov, N. A., Rapoport, V. O., & Tarasov, A. F. (1968). Relation between geomagnetic activity and the sporadic radio emission recorded by the Elektron satellites. *Cosmic Research*, *6*, 791–794. (English translation of Kosmicheskie Issledovaniya).

Benediktov, E. A., Getmantsev, G. G., Sazonov, Y. A., & Tarasov, A. F. (1965). Preliminary results of measurements of the intensity of distributed extraterrestrial radio-frequency emission at 725 and 1525-kHz frequencies by the satellite Elektron-2. *Cosmic Research*, *3*, 492. (English translation of Kosmicheskie Issledovaniya 3, 614–617).

Calvert, W. (1981). The AKR emission cone at low frequencies. *Geophysical Research Letters*, *8*, 1159–1162. https://doi.org/10.1029/GL008i011p01159

Cummer, S. A., Green, J. L., Reinisch, B. W., Fung, S. F., Kaiser, M. L., Pickett, J. S., et al. (2003). Advances in magnetospheric radio wave analysis and tomography. *Advances in Space Research*, *32*, 329–336. https://doi.org/10.1016/s0273-1177(03)90271-7

Dunckel, N., Ficklin, B., Rorden, L., & Helliwell, R. A. (1970). Low frequency noise observed in the distant magnetosphere with Ogo 1. *Journal of Geophysical Research*, *75*, 1854–1862. https://doi.org/10.1029/JA075i010p01854

Ergun, R. E., Carlson, C. W., McFadden, J. P., Delory, G. T., Strangeway, R. J., & Pritchett, P. L. (2000). Electron-cyclotron maser driven by charged-particle acceleration from quasi-static magnetic-field-aligned potentials. *The Astrophysical Journal*, *538*, 456–466. https://doi.org/10.1086/309094

Feldstein, Y. I., & Starkov, G. V. (1967). Dynamic of auroral belt and polar geomagnetic disturbances. *Planetary and Space Science*, *15*, 209–229. https://doi.org/10.1016/0032-0633(67)90190-0

Gallagher, D. L., & Gurnett, D. A. (1979). Auroral kilometric radiation: Time averaged source location. *Journal of Geophysical Research*, *84*, 6501–6509. https://doi.org/10.1029/JA084iA11p06501

Gurnett, D. A. (1974). The earth as a radio source: Terrestrial kilometric radiation. *Journal of Geophysical Research*, *79*, 4227–4238. https://doi.org/10.1029/JA079i028p04227

Gurnett, D. A., Anderson, R. R., Scarf, F. L., Fredricks, R. W., & Smith, E. J. (1979). Initial results from the ISEE-1 and -2 plasma wave investigation. *Space Science Reviews*, *23*, 103–122. https://doi.org/10.1007/BF00174114

Gurnett, D. A., Huff, R. L., & Kirchner, D. L. (1997). The wide-band plasma wave investigation. *Space Science Reviews*, *79*, 195–208. https://doi.org/10.1023/A:1004966823678

Hanasz, J., Panchenko, M., de Feraudy, H., Schreiber, R., & Mogilevsky, M. M. (2003). Occurrence distribution of the auroral kilometric radiation ordinary and extraordinary wave modes. *Journal of Geophysical Research*, *108*(A11), 1408. https://doi.org/10.1029/2002ja009579

Hanasz, J., Schreiber, R., Pickett, J., & de Feraudy, H. (2008). Pulsations of auroral kilometric radiation at Pc1 frequencies. *Geophysical Research Letters*, *35*, L15819. https://doi.org/10.1029/2008gl034609

Huff, R. L., Calvert, W., Craven, J. D., Frank, L. A., & Gurnett, D. A. (1988). Mapping of auroral kilometric radiation sources to the aurora. *Journal of Geophysical Research*, *93*, 11445–11454. https://doi.org/10.1029/JA093iA10p11445

Kurth, W. S., Baumback, M. M., & Gurnett, D. A. (1975). Direction-finding measurements of auroral kilometric radiation. *Journal of Geophysical Research*, *80*(19), 2764–2770. https://doi.org/10.1029/ja080i019p02764

LaBelle, J., Yan, X., Broughton, M., Pasternak, S., Dombrowski, M., Anderson, R. R., et al. (2015). Further evidence for a connection between auroral kilometric radiation and ground-level signals measured in Antarctica. *Journal of Geophysical Research: Space Physics*, *120*(3), 2061–2075. https://doi.org/10.1002/2014ja020977

LaBelle, J., Yearby, K., & Pickett, J. S. (2022). South Pole Station ground-based and Cluster satellite measurements of leaked and escaping Auroral Kilometric Radiation. *Journal of Geophysical Research: Space Physics*, *127*, 2021JA029399. https://doi.org/10.1029/2021JA029399

Louarn, P., Roux, A., de Feraudy, H., Le Quéau, D., André, M., & Matson, L. (1990). Trapped electrons as a free energy source for the auroral kilometric radiation. *Journal of Geophysical Research*, *95*(A5), 5983–5995. https://doi.org/10.1029/ja095ia05p05983

Melrose, D. B. (1976). An interpretation of Jupiter's decametric radiation and the terrestrial kilometric radiation as direct amplified gyroemission. *The Astrophysical Journal*, *207*, 651–662. https://doi.org/10.1086/154532

Menietti, J. D., Mutel, R. L., Santolik, O., Scudder, J. D., Christopher, I. W., & Cook, J. M. (2006). Striated drifting auroral kilometric radiation bursts: Possible stimulation by upward traveling EMIC waves. *Journal of Geophysical Research*, *111*, A04214. https://doi.org/10.1029/2005ja011339

Mutel, R. L., Christopher, I. W., Menietti, J. D., Gurnett, D. A., Pickett, J. S., Masson, A., et al. (2011). RX and Z-mode growth rates and propagation at cavity boundaries. In *Planetary radio emissions VII* (pp. 241–252). Austrian Academy of Sciences.

Mutel, R. L., Christopher, I. W., & Pickett, J. S. (2008). Cluster multispacecraft determination of AKR angular beaming. *Geophysical Research Letters*, *35*, L07104. https://doi.org/10.1029/2008gl033377

Mutel, R. L., Gurnett, D., & Christopher, I. (2004). Spatial and temporal properties of AKR burst emission derived from cluster WBD VLBI studies. *Annales Geophysicae*, *22*, 2625–2632. https://doi.org/10.5194/angeo-22-2625-2004

Mutel, R. L., Gurnett, D. A., Christopher, I. W., Pickett, J. S., & Schlax, M. (2003). Locations of auroral kilometric radiation bursts inferred from multispacecraft wideband cluster VLBI observations: 1. Description of technique and initial results. *Journal of Geophysical Research*, *108*(A11), 1398. https://doi.org/10.1029/2003ja010011

Mutel, R. L., Menietti, J. D., Christopher, I. W., Gurnett, D. A., & Cook, J. M. (2006). Striated auroral kilometric radiation emission: A remote tracer of ion solitary structures. *Journal of Geophysical Research*, *111*, A10203. https://doi.org/10.1029/2006ja011660

Mutel, R. L., Peterson, W. M., Jaeger, T. R., & Scudder, J. D. (2007). Dependence of cyclotron maser instability growth rates on electron velocity distributions and perturbation by solitary waves. *Journal of Geophysical Research*, *112*, A07211. https://doi.org/10.1029/2007ja012442

Parrot, M., & Berthelier, J.-J. (2012). AKR-like emissions observed at low altitude by the DEMETER satellite. *Journal of Geophysical Research*, *117*(A10), A10314. https://doi.org/10.1029/2012ja017937

Pottelette, R., Berthomier, M., & Pickett, J. (2014). Radiation in the neighbourhood of a double layer. *Annales Geophysicae*, *32*, 677–687. https://doi.org/10.5194/angeo-32-677-2014

Pottelette, R., & Pickett, J. (2007). Phase space holes and elementary radiation events. *Nonlinear Processes in Geophysics*, *14*, 735–742. https://doi.org/10.5194/npg-14-735-2007

Pritchett, P. L., Strangeway, R. J., Ergun, R. E., & Carlson, C. W. (2002). Generation and propagation of cyclotron maser emissions in the finite auroral kilometric radiation source cavity. *Journal of Geophysical Research*, *107*, 1437. https://doi.org/10.1029/2002ja009403

Uozumi, T., Yumoto, K., Tokunaga, T., Solovyev, S. I., Shevtsov, B. M., Marshall, R., et al. (2011). AKR modulation and global Pi2 oscillation. *Journal of Geophysical Research*, *116*, A06214. https://doi.org/10.1029/2010ja016042

Wu, C. S., & Lee, L. C. (1979). A theory of the terrestrial kilometric radiation. *The Astrophysical Journal*, *230*, 621–626. https://doi.org/10.1086/157120